Tree Physiology, 2024, **44**, tpae038
https://doi.org/10.1093/treephys/tpae038
Advance access publication date 12 April 2024
Research paper

Coordinated hydraulic traits influence the two phases of time to hydraulic failure in five temperate tree species differing in stomatal stringency

Pierre-André Waite[1,2,3,*,†], Manish Kumar[1,4,*,†], Roman M. Link[1,2], Bernhard Schuldt[1,2]

[1]Julius-von-Sachs-Institute of Biological Sciences, Ecophysiology and Vegetation Ecology, University of Würzburg, Julius-von-Sachs-Platz 3, 97082 Würzburg, Germany
[2]Forest Botany, TUD Dresden University of Technology, Pienner Straße 7, 01737, Tharandt, Germany
[3]CIRAD, UPR AIDA, 34398 Montpellier, France
[4]ICAR - Central Soil Salinity Research Institute (CSSRI), Karnal, 132001, India

*Corresponding authors (waite@plant-ecophysio.com, manish.kumar2@icar.gov.in)

†These authors contributed equally to this work.

Handling Editor: Sebastian Pfautsch

Worldwide, forests are increasingly exposed to extreme droughts causing tree mortality. Because of the complex nature of the mechanisms involved, various traits have been linked to tree drought responses with contrasting results. This may be due to species-specific strategies in regulating water potential, a process that unfolds in two distinct phases: a first phase until stomatal closure, and a second phase until reaching lethal xylem hydraulic thresholds. We conducted dry-down experiments with five broadleaved temperate tree species differing in their degree of isohydry to estimate the time to stomatal closure (t_{sc}) and subsequent time to critical hydraulic failure (t_{crit}). We measured various traits linked to tree drought responses, such as the water potentials at turgor loss point (P_{tlp}), stomatal closure (P_{gs90}), and 12%, 50% and 88% loss of xylem hydraulic conductance (P_{12}, P_{50}, P_{88}), hydraulic capacitance (C), minimum leaf conductance (g_{min}), hydroscape area (HSA) and hydraulic safety margins (HSM). We found that P_{gs90} followed previously recorded patterns of isohydry and was associated with HSA. Species ranked from more to less isohydric in the sequence *Acer pseudoplatanus* < *Betula pendula* < *Tilia cordata* < *Sorbus aucuparia* < *Fagus sylvatica*. Their degree of isohydry was associated with leaf safety (P_{tlp} and g_{min}), drought avoidance (C) and t_{sc}, but decoupled from xylem safety (HSM and P_{88}) and t_{crit}. Regardless of their stomatal stringency, species with wider HSM and lower P_{88} reached critical hydraulic failure later. We conclude that the duration of the first phase is determined by stomatal regulation, while the duration of the second phase is associated with xylem safety. Isohydry is thus linked to water use rather than to drought survival strategies, confirming the proposed use of HSA as a complement to HSM for describing plant drought responses before and after stomatal closure.

Key words: anisohydry, capacitance, cuticular conductance, desiccation time, hydraulic safety margin, hydroscape area, isohydry, stomatal closure, water potential regulation.

Introduction

Drought-induced tree mortality caused by global change-type drought events is widespread and well documented in almost all forest types across the globe (Hammond et al. 2022) including Central Europe (Schuldt et al. 2020). The global increasing evaporative demand has been linked to reductions in biomass productivity and rising tree mortality (Yuan et al. 2019, Grossiord et al. 2020, McDowell et al. 2022). Ultimately, tree mortality during drought depends on how long plants can maintain the integrity of their water transport system and tissue water content to sustain biochemical functionality (Adams et al. 2017, Nolan et al. 2021, Hajek et al. 2022, Mantova et al. 2022).

The progression of plant drought responses can be divided in two fundamental phases, a first phase before stomatal closure when the plant is still actively transpiring, and a second phase from stomatal closure to deadly levels of desiccation (Choat et al. 2018). Before stomatal closure, stomatal regulation is the main driver of plant water loss, as the conductance of open stomata exceeds other water losses by orders of magnitude (Kerstiens, 1996). Under water deficit, stomata gradually close to minimize water loss and xylem water potential drop (Brodribb et al. 2003, Nolf et al. 2015). After stomatal closure, plant water potentials continue to decrease through water losses via the cuticle, bark and residual stomatal conductance, until finally reaching levels that cause the spread of embolism in the xylem (Blackman et al. 2016, Blackman et al. 2019, Hammond and Adams 2019).

Several traits related to the aforementioned processes are routinely quantified to describe plant behaviour under drought. Hydraulic impairment is usually described using xylem embolism thresholds derived from vulnerability curves, such as the water potential at 50% and 88% loss of hydraulic conductivity (P_{50} and P_{88}, respectively; Brodribb and Cochard 2009, Urli et al. 2013). One aspect of plant drought responses is avoiding the onset of xylem embolism formation by adjusting the internal water balance through stomatal regulation (Li et al. 2018). The water potential at 50% or 90% stomatal closure (P_{gs50} and P_{gs90}) has been shown to be positively related to embolism thresholds (P_{50} and P_{88}), and to be positively linked to plant mortality risk during drought (Klein 2014, Bartlett et al. 2016;

Received: July 5, 2023. **Accepted:** March 28, 2024

Martin-StPaul et al. 2017, Li et al. 2018). Likewise, leaf turgor loss point (P_{tlp}) is a good predictor of plant hydraulic safety and stomatal closure (Brodribb et al. 2003, Bartlett et al. 2012*b*, 2016, Rodriguez-Dominguez et al. 2016, Farrell et al. 2017, Martin-StPaul et al. 2017, Manzi et al. 2022, Ziegler et al. 2023). Coordination between the first and the second phase of drought response is described using the hydraulic safety margin (HSM) between leaf water potential at stomatal closure (i.e. P_{gs90}) or turgor loss point (i.e. P_{tlp}) and critical embolism thresholds (e.g. P_{88}; Skelton et al. 2015, Martin-StPaul et al. 2017). Water losses after stomatal closure are driven by cuticular and residual conductance (g_{min}) (Duursma et al. 2019). Altogether, these coordinated leaf and xylem traits influence plant mortality risk, but also allow water deficit periods to be mitigated in multiple ways (Pivovaroff et al. 2015; Hammond and Adams 2019, Hammond et al. 2019). One method of mitigation is provided by plant hydraulic capacitance, i.e. the ability to store water in tissues and gradually release it during increasing drought stress. Capacitance seems to be a key trait that dynamically modulates both hydraulic safety and efficiency (Meinzer et al. 2003, Sperry et al. 2008). Its importance for buffering intense periods of water shortage is unequivocally accepted (Steppe and Lemeur 2007, Vergeynst et al. 2015, Epila et al. 2017, De Baerdemaeker et al. 2018).

Syndromes of traits allow hydraulic strategies to be categorized. One of them is the degree of isohydry, i.e. the stringency of stomatal control during increasing evaporative demand. In drier environments, more isohydric species tend to close their stomata earlier to limit the decrease in xylem water potentials (Tardieu and Simonneau 1998). Isohydric species thus are assumed to delay the onset of xylem embolism formation at the cost of lower carbon uptake and reduced transpirative cooling. In contrast, more anisohydric species maintain their stomata open for longer at the cost of decreasing water potentials, preserving assimilation but increasing embolism risk (Tardieu and Simonneau 1998, Hartmann et al. 2021). Stomatal sensitivity to water potential varies along a continuum (Klein 2014) from more to less stringent stomatal control. However, some species can switch from isohydric to anisohydric behaviour in response to changing conditions (Rogiers et al. 2012, Zhang et al. 2012). For these reasons, the relevance of a dichotomic nomenclature is widely discussed, while a clear definition of the underlying mechanisms is yet to come (Martínez-Vilalta and Garcia-Forner 2017, Hochberg et al. 2018, Feng et al. 2019). In consequence, a large number of metrics have been proposed to quantify the degree of isohydry of a species, for example, stomatal response curves (e.g. Klein 2014), water potentials at given percentages of loss of stomatal conductance (e.g. Chen et al. 2021), the slope of the relationship of midday versus predawn water potential (e.g. Martínez-Vilalta et al. 2014), the water potential difference between stomatal closure and P_{50} (Skelton et al. 2015), or the hydroscape area (HSA; e.g. Fu and Meinzer 2019, Li et al. 2019, Salvi et al. 2022). These uncertainties illustrate the need to incorporate the concept into a more integrative understanding of the coordination of hydraulic traits during drought.

Recent perspectives emphasize the necessity of dynamic frameworks that quantify plant responses, enhancing the predictability of plant behaviour under drier conditions. Hydraulic traits are interrelated, contributing to a sequence of processes that unfold as water potential decreases. In recent years, numerous studies have explored the concept of trait coordination (e.g. Bartlett et al. 2016, Trueba et al. 2019, Ziegler et al. 2023). The sequence of processes translated into traits typically aligns with the two essential drought response phases previously described. As water potential falls, leaves dehydrate until they experience a loss of turgor, followed by a series of other processes: leaf xylem embolisms begin to form, photochemical processes are disrupted and, ultimately, these factors may result in leaf death (Bartlett et al. 2016, Trueba et al. 2019, Ziegler et al. 2023).

While coordinated traits provide more reliable insights into plant performance during drought than isolated traits, there is a pressing need to incorporate these traits into a framework that considers dynamic factors. Cochard (2021) suggested a novel approach, modelling the time until critical hydraulic failure (t_{hf}), examining how external factors, such as temperature, influence this crucial timeline. Likewise, recent dry-down experiments propose to link drought tolerance and avoidance traits with critical timings of plant response to drought (Blackman et al. 2019, Li et al. 2022; Petek-Petrik et al. 2023). The idea behind these experiments is to measure a set of hydraulic traits and to monitor plant water status on replicate plant samples over a period of progressing desiccation to determine the time necessary to exceed critical desiccation thresholds, e.g. time from full hydration to stomatal closure (t_{sc}) or time from stomatal closure to critical hydraulic failure (t_{crit}). Controlled dry-down experiments allow the identification of drivers of the variability in the timing of critical events during plant response to drought (Choat et al. 2018). While most studies have focused on determining the time a plant spends in the second phase of the drying process, from stomatal closure to critical hydraulic failure (t_{crit}; Blackman et al. 2016, 2019, Challis et al. 2022), so far, to our knowledge, there are no studies that focus on the time plants spend in the first phase from full hydration to stomatal closure (t_{sc}).

In the present study, we investigated the drought response and hydraulic strategies of five temperate major and minor broadleaf tree species. We conducted drying-down experiments on potted saplings of the species *Acer pseudoplatanus*, *Betula pendula*, *Fagus sylvatica*, *Sorbus aucuparia* and *Tilia cordata* to quantify their degree of isohydry based on two metrics, the xylem water potential at stomatal closure (P_{gs90}) and the HSA, and to estimate the time to both stomatal closure (t_{sc}) and critical hydraulic failure (t_{crit}). We further measured a set of water potentials associated with critical points throughout the drying process, namely the xylem water potential at the turgor loss point (P_{tlp}) and at catastrophic hydraulic failure (P_{88}). In addition, we measured various traits linked to drought response, such as the HSM, minimum leaf conductance (g_{min}) and hydraulic capacitance (C). The aims of our study are (i) to determine the position of these tree species along the isohydric continuum according to P_{gs90} and HSA, (ii) to test how hydraulic traits are related among themselves and with degree of isohydry and (iii) how the hydraulic traits covered are related to the two phases of drought response, namely t_{sc} and t_{crit}. We hypothesized that (i) P_{gs90} is negatively associated with HSA and consistent with its degree of isohydry, (ii) more isohydric species have higher C, less negative P_{88}, and a wider HSM, (iii) time to stomatal closure (t_{sc}) is associated with stomatal regulation traits (P_{gs90}, P_{tlp}, HSA) and (iv) time to critical hydraulic failure (t_{crit}) is associated with safety traits (g_{min}, HSM, P_{88}

Table 1. Summary of investigated variables with their symbols, units and definition

Symbols	Units	Definition
P_{pd}	MPa	Water potential at predawn between 5:00 and 6:00 h
P_{md}	MPa	Water potential at midday between 11:30 and 12:30 h
P_{88}	MPa	Xylem water potential at an 88% loss of hydraulic conductance
P_{gs90}	MPa	Water potential at 90% loss of maximum stomatal conductance
P_{tlp}	MPa	Water potential at leaf turgor loss point
HSM	MPa	(Stomatal) hydraulic safety margin defined as the difference between P_{gs90} and P_{88}
C	mol kg^{-1} MPa^{-1}	Hydraulic capacitance calculated as the amount of releasable water in the saplings' tissues per unit change in xylem tension and dry mass
HSA	MPa^2	Hydroscape area calculated as the area of the triangle formed between the 1:1 line and the regression line made between P_{pd} and P_{md}
g_{max}	mmol m^{-2} s^{-1}	Maximum leaf stomatal conductance
g_{min}	mmol m^{-2} s^{-1}	Leaf cuticular conductance calculated as the amount of water lost per area and per time (standardized by VPD and atmospherical pressure)
t_{sc}	h mol mol^{-1}	Time to stomatal closure per unit of VPD
t_{sc_stan}	h mol cm^2 mol^{-1} cm^{-3}	Time to stomatal closure per unit of VPD standardized by the ratio of maximum leaf area on each sapling (cm^2) and its maximum amount of water (derived from capacitance curves; cm^3), represents the time it takes for 1 mL of water to evaporate over a unit surface at a unit of VPD
t_{crit}	h mol mol^{-1}	Time to critical hydraulic failure (P_{88}) starting from stomatal closure per unit of VPD
t_{crit_stan}	h mol cm^2 mol^{-1} cm^{-3}	Time to critical level of hydraulic failure starting from stomatal closure per unit of VPD, standardized by the ratio of maximum leaf area on each sapling (cm^2) and its maximum amount of water (derived from capacitance curves; cm^3), represents the time it takes for 1 mL of water to evaporate over a unit surface at a unit of VPD

and C). We chose to interpret C as a safety trait because of its role in buffering time to critical hydraulic failure (Blackman et al. 2016, 2019).

Materials and methods

Species description

Seeds of three species, sycamore maple (*A. pseudoplatanus* L.), silver birch (*B. pendula* Roth) and rowan (*S. aucuparia* L.), were collected and grown in March 2019 at the botanical garden of the University of Würzburg (49° 45′ 53.7552″ N, 9° 55′ 54.6528″ E; cf. Kumar et al. 2022). All measurements on these species took place on ca. 30 ca. 2-year-old saplings per species in July–August 2021 (Table S1, available as Supplementary data at *Tree Physiology* Online). Two other species, European beech (*F. sylvatica* L.) and small-leaved lime (*T. cordata* Mill.), were grown in a nursery near Würzburg from 2019 to 2021 and repotted in January 2022. Measurements took place in July–August 2022. Because most of the studied traits (Table 1) require destructive measurements, we divided individuals into experiments to estimate a maximum of traits at the species level, using different subsets of trees for drying-out experiments and physiological measurements.

In May 2019 (maple, birch and rowan) and January 2022 (beech and lime), the trees were placed in 7.5 L pots in an Eurohum soil mixture (Eurohum Faser, Article no. 12-03200-xx) containing N, P, and K in a proportion of 14, 16, and 18 kg m^{-3}, respectively. The trees grew in the conditions of Würzburg (180 m a.s.l.; mean annual temperature: 10 °C; mean annual precipitation: 625 mm; Deutscher Wetterdienst 2023) and were kept outside during summer and inside a greenhouse during winter. They were frequently watered and fertilized until the start of the measurement campaigns. We divided the tree replicates into subsets for different sets of experiments. The trees for the dry-down experiments were drought-hardened several weeks prior to the experiments by drying them down for a few days and then rehydrating to their previous water status.

The studied species were selected due to their reported contrasting stomatal behaviour. *Fagus sylvatica* and *S. aucuparia* have been described as clearly anisohydric (Vogt 2001, Rötzer et al. 2017, Leuschner et al. 2019, 2022, Leuschner 2020), *A. pseudoplatanus* and *B. pendula* have consistently been described as isohydric (Robson et al. 2015, Leuschner et al. 2019, Beikircher et al. 2021, Kumar et al. 2022), while the classification of the stomatal behaviour of *T. cordata* is mixed, with some studies reporting a fairly isohydric behaviour (Köcher et al. 2009, 2013, Leuschner et al. 2019) and others report a more anisohydric strategy (Moser et al. 2016, Gillner et al. 2017, Moser-Reischl et al. 2019).

Embolism resistance and HSM

To determine the water potential at critical hydraulic failure and thus plant death, we constructed xylem vulnerability curves on additional saplings with the flow-centrifuge method (Cochard et al. 2005). Measurements were performed in 2021 in the framework of our previous study (Kumar et al. 2022) for *A. pseudoplatanus*, *B. pendula* and *S. aucuparia*, and in 2022 for *F. sylvatica* and *T. cordata*. The main stem of 5 to 10 replicates per species was shortened to a length of ca 27 cm under water and, after removal of the bark at both ends, inserted in a custom-made Cavitron rotor chamber attached to a centrifuge (Cavitron device built from customized a Sorvall RC-5C centrifuge), operated with the Cavisoft software (Cavisoft version 5.2.1, University of Bordeaux, Bordeaux, France). Measurements started at a xylem pressure of −0.8 MPa, which was stepwise decreased until reaching a percent loss of hydraulic conductivity (PLC) of at least 90%. Vulnerability curves were fitted using an exponential-sigmoidal model (Pammenter and Vander Willigen 1998) and subsequently used to determine the water potential at 12%, 50% and 88% loss of conductivity (P_{12}, P_{50} and P_{88},

respectively). The latter was used to estimate the HSM as the difference between P_{gs90} and P_{88}.

Shoot hydraulic capacitance

Hydraulic capacitance (C) measurements were made on the complete aboveground fraction of well-watered saplings ($n = 4$ to 5; branch length = 1.0 to 1.2 m, basal diameter = 10 to 14 mm). We followed an updated version of the method described in Li et al. (2018) and Blackman et al. (2019). After storing the plants overnight in a cool and humid environment in opaque plastic bags to ensure full water saturation, shoot samples were cut-off at the root collar and the cut sealed with wax. During the bench dry down, each shoot was weighted at increasing time intervals at 10 mg precision for quantifying water loss. At each time interval (hereafter: drying steps), the water potential of two leaves per shoot was measured using a pressure chamber. Subsequently, shoots were slowly dried down until mass constancy or reaching the maximum water potential measurable by the pressure chamber (−10 MPa). The initial mass at the beginning of the experiment corresponds to the water-saturated mass (SM) and was always above −0.3 MPa, i.e. all measurements started at water saturation. All subsequent weight measurements (i.e. fresh mass or FM) were done at a series of drying steps with increasing drying intervals (e.g. 15 min, 30 min, 1 h, 2 h, 4 h, etc.) defined depending on species identity and measurement conditions. For each drying step, before measuring mass and water potential, shoots were placed in opaque plastic bags holding humidified towels for 30 to 60 min to limit transpiration and equilibrate the water potential. In addition, the mass of the excised leaves at each drying step was documented before water potential measurement and all cut-off and shed leaves were weighted and stored to measure their oven-dried mass (DM). Subsequently, the wood samples were oven-dried at 105 °C for 72 h and the leaf samples at 75 °C for estimating their DM. Based on the shoot fresh mass at each drying step, the mass of the removed leaves and the corresponding DMs, we computed shoot relative water content for each drying step $i > 1$ (at the first step, RWC is equal to 1 by definition):

$$RWC_i = \frac{SM * \prod_1^i \frac{FM_i}{FM_{i-1}} - DM}{SM - DM} \ [g\ g-1] \qquad (1)$$

where FM_i refers to the fresh mass after each drying step before leaf cutting, and FM_{i-1} refers to the fresh mass of the previous drying step after leaves were cut off. To estimate RWC at a given water potential for each species, the relationship between RWC and water potential was modelled with an exponential decay equation. This was done to estimate the moisture release pattern of each species with a better fit than a linear regression (see methods in Li et al. 2018 and Blackman et al. 2019).

To compare species' capacitance values, we fitted a linear regression on the linear portion of the relationship between RWC and water potential after stomatal closure (Figure S1, available as Supplementary data at *Tree Physiology* Online). We used the slope of the relationship to compare species (see methods in Blackman et al. 2019). The slope was then standardized to account for shoot DM:

$$C = \frac{\Delta RWC}{\Delta \Psi} \cdot \frac{SM - DM}{DM} \cdot \frac{1}{M_w} \left[mol\ kg - 1\ MPa - 1\right] \qquad (2)$$

where $\Delta RWC/\Delta\Psi$ is the slope of the relationship between RWC and water potential (g g^{-1} MPa^{-1}) multiplied by the maximum amount of stored water by the shoot (SM–DM, g) and divided by shoot DM (kg). The resulting value (g kg^{-1} MPa^{-1}) was then converted into mol kg^{-1} MPa^{-1} by dividing it by the molar mass of water (M_w; 18.01 g mol^{-1}).

Drying-out experiments

At the start of the dry-down period in 2021 and 2022, the saplings (see Table S1, available as Supplementary data at *Tree Physiology* Online for details) were irrigated to soil saturation. The pots were then covered with black polythene to reduce evaporation from the topsoil and to ensure that water loss is driven by transpiration only. We installed a microclimate sensor (1-800-LOGGER, HOBO Onset, Bourne, MA, USA) just above the saplings (height = 1.3 m) to record air temperature and humidity every 10 min. Irrigation was then suspended, allowing a progressive decrease in water potential until the plants reached their P_{88} (measured on conspecific saplings from the same batch of plants prior to the experiment). We monitored predawn leaf water potential regularly with a pressure chamber (Model 1505D, PMS Instruments, Albany, OR, USA). We selected each one leaf per individual at predawn (P_{pd}, MPa; from 5 to 6 a.m.) and midday (P_{md}, MPa; from 12 a.m. to 1 p.m.), and measured water potential within 1 min after excision. Throughout the experiment, we observed a reduction of the total leaf area (encompassing sampled and shed leaves) ranging from 1.62% to 13.07% for *S. aucuparia* and *T. cordata*, respectively, with the other species experiencing a loss under 4%.

During the dry-out period, all leaves lost due to measurements or leaf shedding were collected and oven-dried at 75 °C for 72 h to estimate the initial leaf mass and area of each sapling and its change over time. We also oven-dried the saplings at 75 °C at the end of the experiments to estimate their aboveground stem and leaf mass. We obtained leaf area per plant by multiplying leaf DM (g) by species specific leaf area (SLA, cm^2 g^{-1}) measured on different fully hydrated saplings (from the same batch). Total leaf area (A_{leaf}, cm^2) of the dried-out saplings was estimated from SLA based on the sum of the DM of the leaves removed daily and the DM of the leaves remaining at the end of the experiment. Likewise, we obtained the amount of water stored in the aboveground fraction of the dried-out plants (V_w, g) by multiplying total aboveground DM (i.e. removed + remaining leaves + stems, in g) with species saturated shoot water content (g g^{-1}) obtained during the capacitance experiment. Species-level saturated water content was measured on saplings used for hydraulic capacitance measurements as (wet mass − dry mass)/dry mass.

Plant stomatal response during drought

Stomatal conductance (g_s, mmol m^{-2} s^{-1}) was measured on drying plants to estimate the water potential at stomatal closure, i.e. the water potential at 90% loss of stomatal conductance (P_{gs90}). On each tree, three fully expanded, healthy

leaves were selected at different relative positions along the stem (i.e. top, middle and lower) and permanently marked for repeated measurements of g_s during the same time of each day using a portable porometer (model AP4, Delta-T Devices Ltd, Cambridge, UK). Measurement started every morning at 9 a.m. after calibrating the porometer according to the manufacturer's guidelines. We subsequently measured g_s on all designated leaves, typically comprising 10–15 leaves per species. Between measurement sessions, we calibrated the device again in case there were notable deviations in temperature and humidity since the previous calibration. We then measured all marked leaves again in the same order. In 2021, we monitored g_s of *S. aucuparia*, *A. pseudoplatanus* and *B. pendula* through four sessions spanning from 9 a.m. to 3 p.m. on the initial 2 days to identify the time of maximum stomatal conductance. We reduced it to two morning sessions for the subsequent 8 days, during peak photosynthetic activity between 9 a.m. and 10 a.m. For *F. sylvatica* and *T. cordata* in 2022, our measurements were confined to two morning sessions spanning 9 days during peak stomatal activity.

We computed percent of stomatal conductance using the highest recorded individual g_s as reference. Finally, we estimated species stomatal response to drought by fitting a sigmoidal curve on the relationship between percent of stomatal conductance and water potential (Li et al. 2018).

Determination of plant desiccation times

We defined time to hydraulic failure (t_{hf}) as the species average standardized time to reach the water potential at an 88% loss of hydraulic conductivity starting from a fully hydrated state. t_{hf} was determined for each species by fitting a linear relationship between the observed standardized drying time (i.e. time in hours multiplied by daily average vapour pressure deficit (VPD) to account for differences in evaporative demand across the drying-out experiments) and predawn water potential (P_{pd}) of the dried-out trees. In the present study, for consistency with Blackman et al. (2019), we consider an individual as hydraulically dead when P_{pd} reached P_{88}, since it is described as the threshold of irreversible drought damage in angiosperms (Urli et al. 2013). We divided t_{hf} into the time to stomatal closure (t_{sc}) and the time from stomatal closure to critical hydraulic failure (t_{crit}; Blackman et al. 2016, 2019). Because plant size influences desiccation time (Blackman et al. 2019, Challis et al. 2022), we further standardized t_{sc} and t_{crit} to account for leaf area and water storage (Eq. 3):

$$t_{x\_stan} = t_x \cdot \frac{L_m \cdot \rho_w}{V_w} \quad (3)$$

where t_{x_stan} is the standardized desiccation time x (h cm^{-1}), t_x is the desiccation time for the same tree in VPD hours (mol mol^{-1} h), L_m (cm^2) is its initial leaf area and V_w (g) is the mass of water stored in the wood. V_w was divided by the density of water ρ_w (i.e. 0.996 g cm^{-3} at 30 °C) to convert it to cm^3 (cf. Challis et al. 2022).

Hydroscape area

To estimate species' HSA (MPa^2), we followed the methodology described by Meinzer et al. (2016). Briefly, we calculated HSA as the area of the triangle formed by the regression line between P_{pd} versus P_{md} and the 1:1 line (Eq. 4):

$$\text{HSA} = \frac{a \times b}{2} \quad (4)$$

where a is the intercept of the ordinary linear regression of P_{pd} versus P_{md}, which represents the most negative P_{md} when $P_{pd} = 0$, and b is the intersection of P_{pd} versus P_{md} and the 1:1 line, which is at $P_{pd} = P_{md}$. It is important to note that we excluded water potential values collected the first days under humid conditions when P_{MD} likely varied independently of P_{PD} (Fu and Meinzer 2019).

Leaf traits

On additional well-watered saplings, we measured the water potential at leaf turgor loss point (P_{tlp}), SLA and leaf cuticular conductance (g_{min}) on fully expanded leaves from different canopy positions.

P_{tlp} was estimated using two to three leaves from fully hydrated saplings ($n = 4$ individuals per species) following Bartlett et al. (2012*a*). The leaves were cut-off, cleaned, double-bagged with humidified towels, and stored at 4 °C until measurement. Subsequently, leaf discs were cut out, covered with aluminium foil and submerged in liquid nitrogen for at least 2 min before measuring osmolality (mmol kg^{-1}) with a vapour pressure osmometer (VAPRO 5600, Wescor, USA), which was used to estimate P_{tlp} according to Bartlett et al. (2012*a*).

SLA (cm^2 g^{-1}) was measured on 10 to 30 leaves from fully hydrated saplings ($n = 5$ per species). To compute the SLA, we divided the leaf surface area (cm^2) computed from scans using ImageJ by their oven-dried mass (g).

g_{min} was measured on two to three mature, healthy leaves from the saplings used for capacitance measurements. Excised leaves were cleaned and rehydrated overnight by immersing their petioles in water before recording their saturated leaf mass at 0.1 mg precision and sealing the cut with wax. Leaves were bench-desiccated for 7–10 h while documenting temperature and relative humidity. Fresh mass was recorded at 30 min intervals. Subsequently, samples oven-dried at 70 °C for 48 h after scanning the leaves in order to calculate the leaf area using ImageJ. The projected leaf area was multiplied by two to account for total leaf surface. The transpiration rate J (mmol m^{-2} s^{-1}) was approximated as the slope of the linear regression between leaf mass and time (g s^{-1}; see Sack and Scoffoni 2011), divided by the leaf area (m^2) and the millimolar mass of water (1.8015×10^{-2} g mmol^{-1}). Cuticular conductance g_{min} (mmol m^{-2} s^{-1}) was then calculated as $g_{min} = J \times P_{amb}/\text{VPD}$, where P_{amb} is the ambient pressure (kPa), VPD is the vapour pressure deficit (kPa) and their ratio VPD/P_{amb} is the difference in mole fraction of water vapour inside and outside the leaf as the driving force of diffusion over the leaf surface assuming water vapour saturation in the mesophyll (cf. Nobel 2009, pp 379f).

Data analysis

All data visualizations and statistical analyses were performed using R (version 4.1.2, R Development Core Team 2021). We computed vulnerability and stomatal response curves using the classic sigmoidal model by Pammenter and Vander Willigen (1998) and t_{hf}, t_{sc}, t_{crit}, C and g_{min} using linear models from base R (for more details see previous corresponding sections).

We compared characteristics across species using one-way ANOVA and post hoc tests (Tukey's HSD) for pairwise comparisons using the package `multcompView` (Graves et al. 2023). Subsequently, we assessed associations between traits based on a Pearson correlation matrix plotted with R package

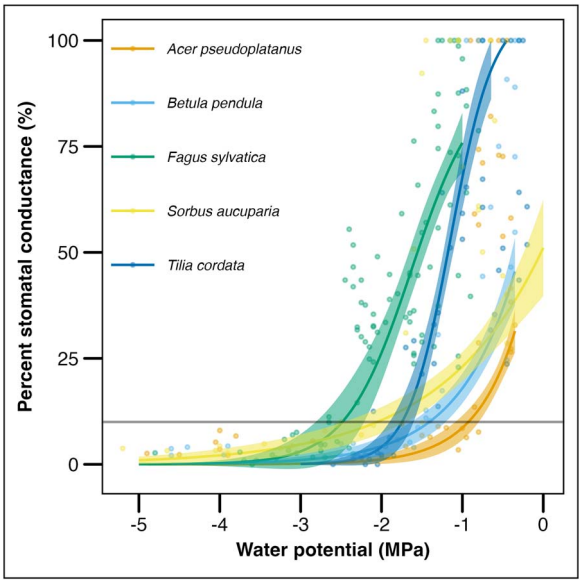

Figure 1. Stomatal response curves of dried-out saplings from the five investigated temperate tree species ($n = 4$ to 5). Presented are percentage of maximal stomatal conductance measured daily until complete stomatal closure against leaf water potential. Fitted lines and 95% confidence intervals (coloured ribbons) were calculated using a sigmoidal equation. Water potential at a 90% loss of stomatal conductance (P_{gs90}) is represented by the horizontal grey line.

corrmorant v0.0.0.9007 (R Link 2020). Due to the necessity of destructive sampling for some methods, analyses of trait associations on the individual level are not possible. The small sample of species in our study result in weak evidence for specific trait–trait associations. We therefore focus on the patterns of covariance among multiple traits. To identify patterns in the correlations between the traits, we performed a hierarchical clustering on the correlation matrix using base R function `hclust()` with the complete linkage method after converting the correlation matrix into a dissimilarity matrix by subtracting the absolute correlations from 1. We then tested if the first split of this clustering explained a significant fraction of the patterns in the correlations by performing a permutational multivariate analysis of variance on the aforementioned dissimilarity matrix using R function `adonis2()` from `vegan` v.2.6-4 (Oksanen et al. 2022) with 10,000 permutations. To compare the clustering based grouping against the grouping from our hypotheses, we made an analogous test for the groups of variables defined in hypotheses (iii) and (iv).

Finally, we performed a principal component analysis (PCA) on the same traits to examine the multivariate association among the different traits using base R and illustrated it using the package `ggbiplot`.

Results

Species stomatal behaviour and relative degree of isohydry

Stomatal conductance (g_s) varied considerably across species and, after experimentally controlling for measurement time by performing measurements at the same time each day, was driven by leaf water potential decline (Figure 1; Table 2). Maximum g_s was particularly high in *F. sylvatica*, *T. cordata* and *S. aucuparia* (species previously described as

Table 2. Hydraulic properties of the five investigated temperate tree species. Provided are stomatal stringency categories as described in previous studies (see Materials and methods section), standardized time to stomatal closure (t_{sc_stan}, h mol mol^{-1} cm^2 cm^{-3}), standardized time to critical hydraulic failure (P_{88}) starting from stomatal closure (t_{crit_stan}, h mol mol^{-1} cm^2 cm^{-3}), standardized time to hydraulic failure (t_{hf_stan}, h mol mol^{-1} cm^2 cm^{-3}), water potential at turgor loss point (P_{tlp}, MPa), water potential at 90% loss of stomatal conductance (P_{gs90}, MPa), water potential at an 88% loss of hydraulic conductance (P_{88}, MPa), HSM ($P_{gs90} - P_{88}$, MPa), HSA (MPa^2), standardized branch hydraulic capacitance (C, mol kg^{-1} MPa^{-1}) and leaf cuticular conductance (g_{min}, mmol m^{-2} s^{-1}).

Species	Stomatal stringency	t_{sc_stan}	t_{crit_stan}	t_{hf_stan}	P_{tlp}	P_{gs90}	P_{12}	P_{88}	HSM	HSA	C	g_{min}	g_{max}
Acer pseudoplatanus	Isohydric[1,5,6,11]	60.52 ± 6.36	32.05 ± 4.33	92.57 ± 6.94	−2.05 ± 0.05	−0.93 ± 0.08	−2.99 ± 0.11	−4.24 ± 0.13	3.31	0.26 ± 0.03	5.33 ± 1.34	3.33 ± 0.36	425.00
Betula pendula	Isohydric[1,5,6,11]	52.65 ± 2.98	17.34 ± 3.19	69.99 ± 4.31	−2.10 ± 0.06	−1.41 ± 0.11	−1.72 ± 0.05	−2.21 ± 0.04	0.80	0.39 ± 0.05	10.98 ± 2.31	1.82 ± 0.16	500.00
Tilia cordata	Isohydric[3,4,6]/Anisohydric[2,9,10]	71.82 ± 10.51	34.64 ± 5.13	106.45 ± 10.13	−1.96 ± 0.09	−1.75 ± 0.09	−2.65 ± 0.21	−4.20 ± 0.13	2.45	1.17 ± 0.06	7.09 ± 0.26	1.28 ± 0.09	229.00
Sorbus aucuparia	Anisohydric[6,7,8,12,13]	48.03 ± 2.59	29.88 ± 3.20	77.91 ± 4.98	−2.37 ± 0.08	−2.05 ± 0.20	−2.73 ± 0.08	−5.02 ± 0.12	2.97	1.73 ± 0.69	4.76 ± 0.67	1.73 ± 0.28	560.00
Fagus sylvatica	Anisohydric[6,7,8,12,13]	84.52 ± 8.80	18.37 ± 2.04	102.89 ± 9.07	−2.48 ± 0.07	−2.49 ± 0.14	−3.09 ± 0.22	−4.10 ± 0.19	1.61	1.85 ± 0.12	2.47 ± 0.40	1.65 ± 0.09	109.00

[1]Beikircher et al. (2021). [2]Gillner et al. (2017). [3]Köcher et al. (2009). [4]Köcher et al. (2013). [5]Kumar et al. (2022). [6]Leuschner et al. (2019). [7]Leuschner (2020). [8]Leuschner et al. (2022). [9]Moser et al. (2016). [10]Moser-Reischl et al. (2019). [11]Robson et al. (2015). [12]Rötzer et al. (2017). [13]Vogt (2001). Given values are means ± SE for each species ($n = 4$ to 8 saplings).

anisohydric; Figure 1) and decreased more slowly alongside water potential than for *B. pendula* and *A. pseudoplatanus* (species described as isohydric). Likewise, the estimated the water potential at 90% loss of stomatal conductance (P_{gs90}) mirrored previously recorded patterns of isohydry, with more negative P_{gs90} values for less isohydric species (Table 2). Moreover, more isohydric species closed their stomata well before reaching the water potential at stomatal closure (P_{tlp}), while P_{gs90} coincided well with P_{tlp} in less isohydric species (Table 2).

In addition, the three species positioned on the more anisohydric end of the spectrum had an HSA > 1, while the more isohydric species had a much lower HSA (Figure 2; Table 2). We recorded a 6-fold difference between the two most extreme HSA (0.29 and 1.85 MPa^2 for *A. pseudoplatanus* and *F. sylvatica*, respectively), which showed a similarly pronounced variation across species as P_{gs90} (Table 2). As expected, HSA was strongly and linearly associated with P_{gs90} (Figure S2, available as Supplementary data at *Tree Physiology* Online; $R^2 = 0.91$, $P = 0.01$), and resulted in the same ranking of species.

Coordination among hydraulic traits

We found that both branch and leaf traits differed significantly across the five species (ANOVA, $P < 0.001$; Figure 3; Table 2). Along a sequence of water potentials, hydraulic traits were well coordinated. For four species, P_{tlp} was reached before onset of embolism (P_{12}, Table 2), while for *B. pendula*, it happened before P_{50} but after P_{12}. Species also closed their stomata at similar water potentials or before losing their leaf turgor (Table 2, P_{tlp} and P_{s90} in Figure 4).

In the investigated species, there is only a weak link between xylem and leaf traits (P_{tlp} and P_{88} in Figure 4), with more embolism resistant species also tending to have a more negative P_{tlp}. Finally, hydraulic capacitance measured on all aboveground tissues was primarily linked to leaf safety and mildly to xylem safety (*C* with P_{tlp} and P_{88} in Figure 4). Species with a higher hydraulic capacitance tended to be more vulnerable to drought-induced embolism and to lose their leaf turgor at less negative water potentials.

Coordination between traits and the degree of isohydry

We found that the degree of isohydry of a species, as quantified by P_{gs90} and HSA, was most strongly associated with leaf traits (e.g. P_{tlp} and g_{min}) and drought avoidance traits (e.g. C; Figures 3 and 4). The lowest *C* was recorded for the most anisohydric species (mean ± SE of 2.47 ± 0.40 and 4.76 ± 0.67 mol kg^{-1} MPa^{-1} for *F. sylvatica* and *S. aucuparia*, respectively; Figure 3), while the highest *C* was recorded for one of the most isohydric species (10.98 ± 2.31 mol kg^{-1} MPa^{-1} for *B. pendula*; Figure 3). On the contrary, less isohydric species presented the most negative P_{88}, while the least negative P_{88} was found for *B. pendula* (−2.21 ± 0.04 MPa; Figure 3). P_{tlp} was the lowest for the least isohydric species (−2.48 ± 0.07 and − 2.37 ± 0.08 MPa for *F. sylvatica* and *S. aucuparia*, respectively; Figure 3).

Overall, we found well-defined general patterns linking the coordinated hydraulic traits with species' degree of isohydry. In our species sample, we could associate a late stomatal closure at low leaf water potentials with a large HSA, i.e. more anisohydric species had a more negative P_{tlp}, lower g_{min} and lower *C* (Figure 4). Likewise, those species had a more negative P_{88}, although they did not possess a wider HSM.

Coordination among traits, the degree of isohydry and critical timings until hydraulic failure

Our drying out experiments revealed a broad range in the time to complete hydraulic failure (t_{hf}; Figure S3, available as Supplementary data at *Tree Physiology* Online). The unstandardized t_{hf} ranged from 464 VPD hours (i.e. time adjusted by daily VPD) for *A. pseudoplatanus* to 282 VPD hours for *B. pendula*, which appeared independent of the species-specific degree of isohydry. After accounting for differences in plant size and total leaf area, *T. cordata* and *F. sylvatica* emerged as the species reaching t_{hf} latest, while *B. pendula* and *S. aucuparia* reached hydraulic failure first. This is well represented by the aggregation of standardized time to stomatal closure (t_{sc}) and time to critical hydraulic failure (t_{crit}, Figure 5). The higher the aggregated value, i.e. t_{hf}, the longer it took to reach P_{88} after accounting for differences in size (Figure 5). Even after standardization, t_{hf} seemed independent of species degree of isohydry. The contribution of the time to stomatal closure (t_{sc_stan}) to the total time to hydraulic failure (t_{hf_stan}) was larger than the contribution of the time from P_{gs90} to P_{88} (t_{crit_stan}) for all species (ranging from 62% to 85%; Figure 5, Table 2) As expected, with 16%, the t_{crit_stan} contribution to t_{hf_stan} was the lowest in *F. sylvatica*.

We found that as expected in hypotheses (iii) and (iv), the correlations between traits and drying times clustered in two groups, one of which containing t_{sc_stan} and stomatal regulation traits, and the other containing t_{crit_stan} and xylem safety traits (Figure 4). However, contrary to our expectation, both hydraulic capacitance and g_{min} were more strongly associated with the first cluster containing t_{sc_stan} than with the second cluster containing t_{crit_stan}. While our initial grouping (iii) and (iv) only explained a marginally significant fraction of the partitioning of the correlations (dissimilarity-based permutational multivariate ANOVA, $P = 0.0836$, $F_{1,7} = 3.04$, $R^2 = 0.302$), the grouping based on the hierarchical clustering (grey areas in Figure 4) resulted in a considerable improvement ($P = 0.0097$, $F_{1,7} = 8.18$, $R^2 = 0.534$). Specifically, we found that less isohydric species were taking longer to completely close their stomata (P_{gs90} and t_{sc_stan} in Figure 4). While t_{sc_stan} appeared largely decoupled from most other investigated characteristics, t_{crit_stan} was highly related with safety traits at the wood (i.e. with P_{88}, Figure 4), at the leaf (i.e. with P_{tlp}) and at the plant level (i.e. with HSM). Interestingly, t_{hf_stan} alone remained mostly unrelated to other hydraulic traits (Table S2, available as Supplementary data at *Tree Physiology* Online), highlighting the importance of dividing plant response to drought into phases representing different processes.

The coordination between hydraulic traits, isohydry metrics and drying times can be observed in the PCA biplot in Figure 6. The observed traits cluster along two main axes of variation that reflect their association with the different phases. The two primary axes of traits variability collectively explained 74.5% of the total variation in the dataset (Table S3, available as Supplementary data at *Tree Physiology* Online). The first PCA axis (PC1) is linked to traits associated with stomatal stringency and plant isohydric behaviour and reflects that species with larger HSA close their stomata and lose their leaf turgor at a more negative water potential, resulting in

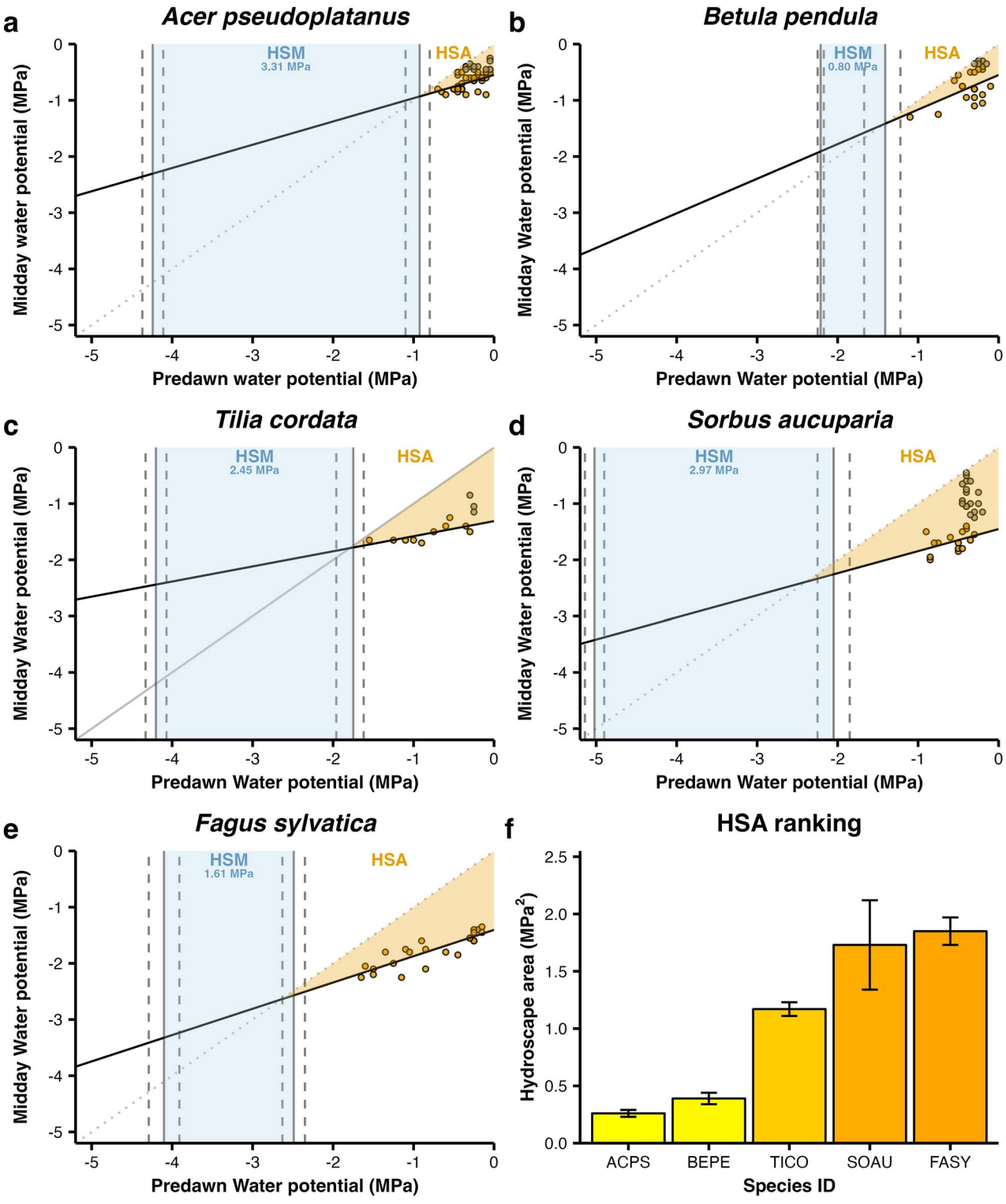

Figure 2. (a–e) Plots of leaf water potential at predawn (P_{pd}; MPa) versus midday (P_{md}; MPa) associated with the 1:1 line for each five investigated temperate tree species ranked by HSA ($n = 5$ to 8). Each point represents one measurement day on one plant with P_{pd} measured before 6:00 h against P_{md} measured between 11:30 and 13:30 h. Orange points were included in the linear regression, while grey points were excluded as they represent data collected under humid conditions when P_{md} likely varied independently of P_{pd} (Fu and Meinzer 2019). The HSA (MPa^2) coloured in light orange was calculated from the area of the triangle formed by the regression line between P_{pd} versus P_{md} and the 1:1 line. Data points beyond $P_{pd} = P_{md}$ were removed according to Meinzer et al. (2016). Species water potential at a 90% loss of stomatal conductance (P_{gs90}; MPa) and at an 88% loss of hydraulic conductivity (P_{88}; MPa) are represented by vertical full lines (± SE = dashed lines). The HSM ($P_{gs90} - P_{88}$; MPa) is coloured in light blue. (f) Barplot of each species' HSA arranged from the narrowest to the widest area. Yellow to orange shades represent an increase in the area and vertical lines represent standard errors (SE). Species abbreviations are as follows: ACPS, *Acer pseudoplatanus*; BEPE, *Betula pendula*; SOAU, *Sorbus aucuparia*; FASY, *Fagus sylvatica*; TICO, *Tilia cordata*.

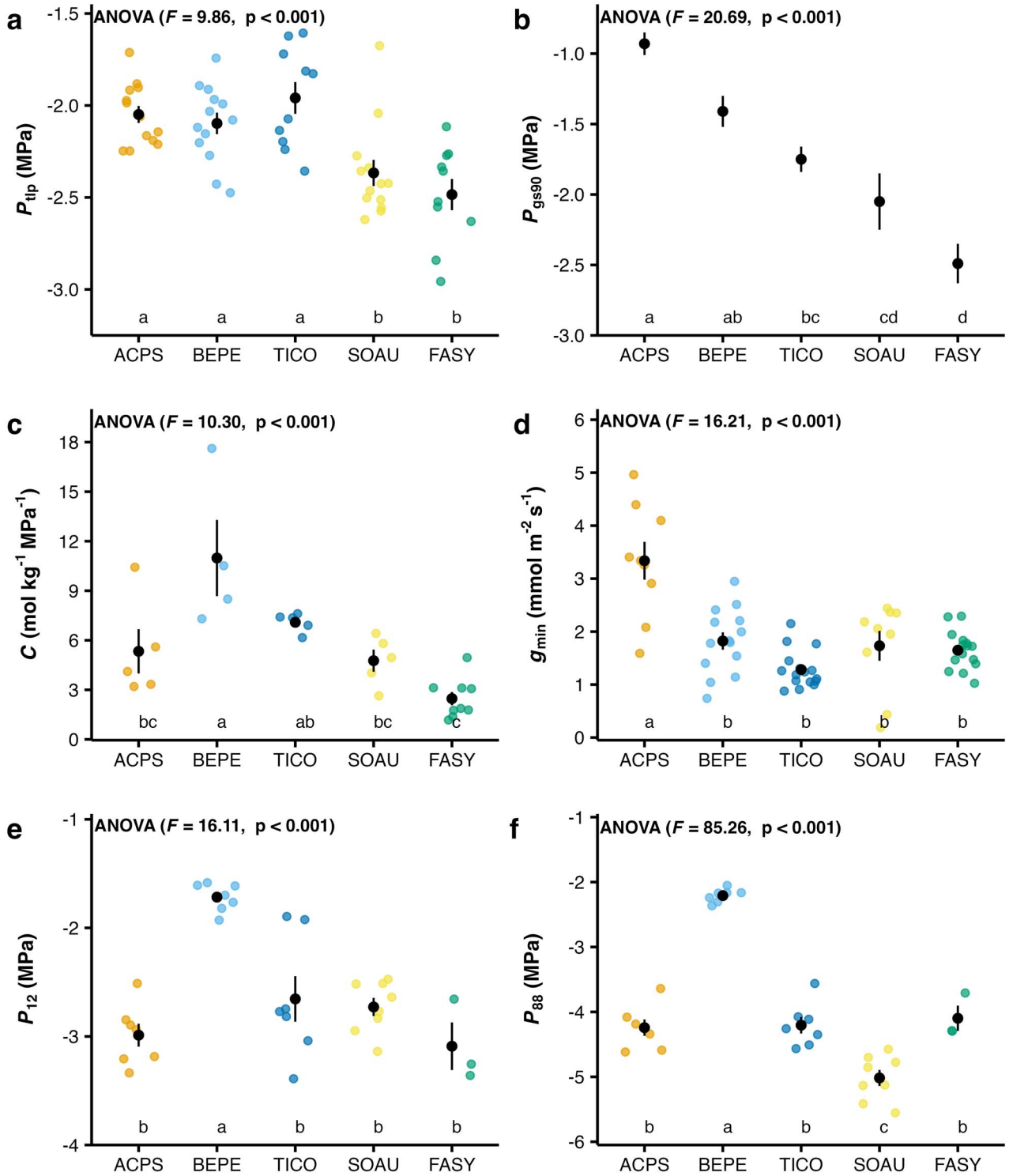

Figure 3. Point and range plots of six hydraulic traits across five temperate tree species. Presented here are (a) leaf water potential at turgor loss point (P_{tlp}), and (b) at a 90% loss of stomatal conductance (P_{gs90}), (c) aboveground shoot hydraulic capacitance (C), (d) leaf cuticular conductance (g_{min}), and xylem water potentials at (e) 12% (P_{12}) and (f) 88% loss of hydraulic conductivity (P_{88}) for each species. Coloured points represent individual measurements done on the entire aboveground part of saplings (C, $n = 5$ to 8), on the main stem (P_{12}, P_{88}, $n = 4$ to 8) or on healthy sun-exposed leaves (P_{tlp} and g_{min}, $n = 8$ to 13). No individual measurement point exists for P_{gs90} since the variable was computed at a species level. Black points represent means ± SE. Significant differences across species were estimated using one-way ANOVA (F-statistic and P-values are given on the top left-hand side of each panel) and post-hoc tests (Tukey HSD, represented by letters). For species abbreviations, see Figure 2.

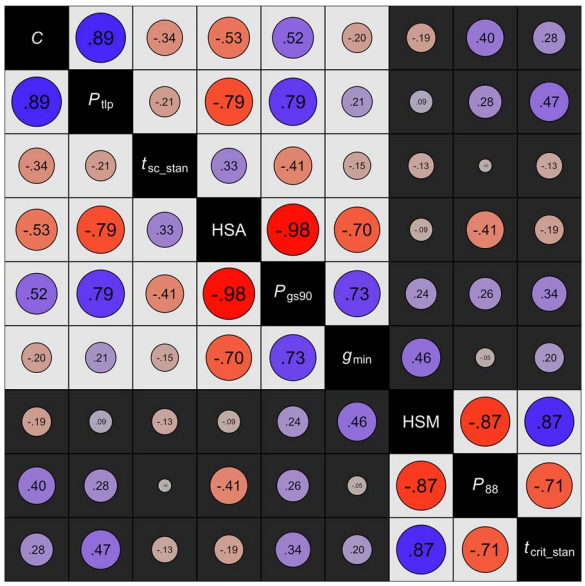

Figure 4. Correlation matrix of investigated hydraulic traits and drying-out threshold times. Presented here are time to stomatal closure (t_{sc_stan}), time to critical water potential (t_{crit_stan}), shoot hydraulic capacitance (C), water potential at an 88% loss of hydraulic conductivity (P_{88}), at the leaf turgor loss point (P_{tlp}) and at a 90% loss of stomatal conductance (P_{gs90}), as well as leaf cuticular conductance (g_{min}), HSM and HSA. The order of the variables is based on hierarchical clustering, the grey areas represent the first split of the clustering. Refer to Table 1 for units and definitions.

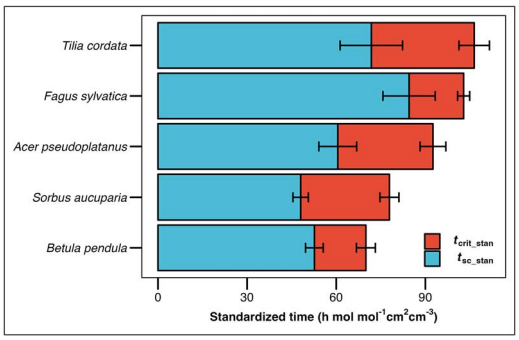

Figure 5. Stacked bar chart depicting time to hydraulic failure divided into two main phases: time to stomatal closure (t_{sc_stan}; h mol mol^{-1} cm^2 cm^{-3}) and time to critical water potential after stomatal closure (t_{crit_stan}; h mol mol^{-1} cm^2 cm^{-3}). To account for climatic conditions and sapling differences, the cumulative times were standardized by the VPD divided by the atmospheric pressure (Mol mol^{-1}), the ratio of maximum leaf area on each sapling (cm^2) and each sapling's maximum amount of water (cm^3). Each threshold time represents the time it takes for 1 ml of water to evaporate over a unit surface at a unit of VPD. Represented here are species mean t_{sc_stan} (± SE; in blue) and t_{crit_stan} (± SE; in red). The percentage of time each species spent within the first phase of drought response (in red) are 65.4% for *A. pseudoplatanus*, 75.2% for *B. pendula*, 67.5% for *T. cordata*, 61.6% for *S. aucuparia* and 84.5% for *F. sylvatica*.

a longer time until stomatal closure. The second PCA axis (PC2) is associated with xylem safety and reflects that species with wider HSM and a more negative P_{88} take longer to reach critical levels of hydraulic failure. Finally, hydraulic capacitance and cuticular conductance seem to be associated with both stomatal stringency and hydraulic safety, however with a tendency for species closing their stomata later to have lower C and g_{min}, as shown in Figure 4.

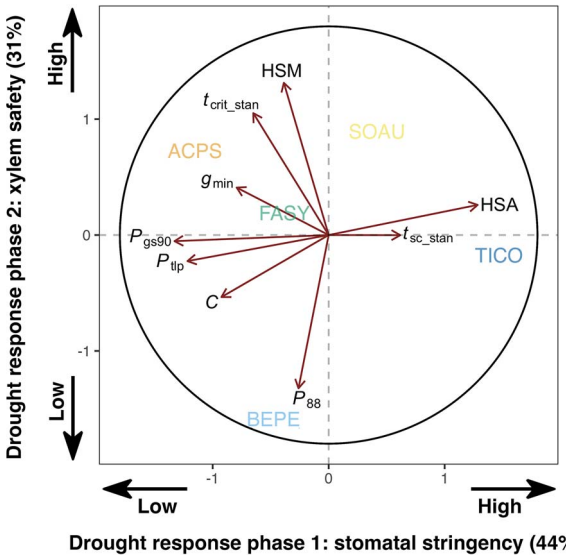

Figure 6. PCA of nine hydraulic characteristics across five temperate tree species. The *x*- and *y*-axes represent species stomatal stringency (i.e. degree of isohydry) and xylem hydraulic safety, respectively. Presented here are standardized times to stomatal closure (t_{sc_stan}), and to critical water potential starting from stomatal closure (t_{crit_stan}), shoot hydraulic capacitance (C), water potential at an 88% loss of hydraulic conductivity (P_{88}), at the leaf turgor loss point (P_{tlp}) and at a 90% loss of stomatal conductance (P_{gs90}), as well as leaf cuticular conductance (g_{min}), HSM and HSA. Refer to Table 1 for units and definitions.

Discussion

The results of this study are consistent with the assumption that plant responses to drought are divided into two discrete phases, the first one lasting from the onset of drought to stomatal closure and the second one from stomatal closure to plant death. We find that the duration of the first phase is mostly influenced by traits related to stomatal regulation, while the duration of the second phase seem to be associated with traits related to xylem resistance. Our results suggest a coordination of drought response traits along two major axes related to these two phases. We further find that the degree of isohydry of a plant is predominantly associated with the first axis linked to the time to stomatal closure, but largely unrelated to the time to critical hydraulic failure. This supports the idea that iso- and anisohydric behaviours are linked to water use strategies rather than to drought survival strategies.

Metrics of the degree of isohydry

To quantify the degree of isohydry of plants, a large number of different metrics have been developed that often result in contrasting results (Martínez-Vilalta and Garcia-Forner 2017, Feng et al. 2019). Here, we found a high correlation between two common metrics of isohydry, the HSA (Meinzer et al. 2016) and the water potential at stomatal closure (cf. Chen et al. 2021). This relationship is in line with previous assessments of the HSA (Li et al. 2019) and illustrates that the latter indeed reflects how stomatal response regulates water potential during drought events, highlighting its value as a general metric of isohydry. However, mapping hydroscapes requires continuous monitoring of plant water potentials during drought events, which is associated with a high measurement effort and can be challenging under field conditions.

While the measurement of stomatal response curves can be achieved over shorter time scales, the required measurement effort is still substantial. Moreover, stomatal conductance not only depends on water potential, but is also sensitive to temperature, light intensity, VPD and thus abscisic acid (ABA) concentrations (Brodribb and McAdam 2017; Klein, 2014), which can induce a high uncertainty in P_{gs90} estimates if not measured under appropriately controlled conditions. For these reasons, measuring isohydry metrics like the HSA or P_{gs90} for large numbers of species remains challenging.

In the last decade, the need for easily measurable traits describing leaf-level drought adaptations has led to a resurgence of interest in pressure-volume curve traits such as the water potential at turgor loss point (Bartlett et al. 2012*b*, 2014). P_{tlp} can be estimated rapidly based on leaf osmometry (cf. Bartlett et al. 2012*a*), has an immediate mechanistic importance and has been shown to be strongly associated with parameters of stomatal response curves (Bartlett et al. 2016). Due to its often high correlation with other isohydry metrics like the HSA, P_{tlp} has been proposed as a robust proxy of isohydry (Meinzer et al. 2016, Fu and Meinzer 2019). Leaf turgor is directly involved in passive pathways of stomatal closure, as stomatal closure is driven by guard cell turgor, which induces ABA synthesis (McAdam and Brodribb 2014, McAdam et al. 2016). Indeed, recent work indicates that turgor-mediated control of stomatal response is central for the stomatal closure of most woody plants (Rodriguez-Dominguez et al. 2016). The close mechanistic link to stomatal control is reflected in the strong association of P_{tlp} with both P_{gs90} and HSA found in our study, which corroborates the value of P_{tlp} estimates as an easily measurable, mechanistically proximate trait directly linked to stomatal response.

In a study of plant drought responses of species from the Cape region, Skelton et al. (2015) proposed the water potential range between stomatal closure and P_{50} as a further metric of isohydry that merges stomatal and xylem hydraulic strategies. This metric is essentially a stomatal HSM (cf. Martin-StPaul et al. 2017, Li et al. 2019). While the HSM reported here was based on the water potential at 88% loss of hydraulic conductance (P_{88}) to match the definition of time to critical hydraulic failure (t_{crit}), there was no significant association between either the HSM based on the water potential at a 50% loss of hydraulic conductance (P_{50}) and P_{88} with any of the variables associated with the isohydry spectrum. Rather, HSM was related to xylem resistance traits and the duration of the second phase of drought response. Accordingly, stomatal HSMs may not be ideal to describe the stringency of stomatal response. Rather, our results support the proposed use of the HSA as a complement to the HSM to describe plant drought responses before and after stomatal closure (Hartmann et al. 2021).

Despite the evolution and refinement of methodologies to discern plant isohydry, the observed patterns in stomatal response of the studied species, rooted in a more nuanced approach, still converge with traditional literature. Previous studies, using a dichotomous classification, identified species like *F. sylvatica* and *S. aucuparia* as anisohydric. Our research aligns with this characterization, showcasing these species as the least isohydric within our dataset. Similarly, *A. pseudoplatanus* and *B. pendula* have been traditionally marked as robustly isohydric, an observation consistent with our results. Contrasting these, *T. cordata* has received mixed classifications in the past (anisohydric by Moser et al. 2016, Gillner et al. 2017, Kiorapostolou et al. 2018; or isohydric by Leuschner et al. 2019), and presents itself in our study with an intermediate isohydric behaviour. Our results are more in line with Leuschner et al. (2019), who reported fairly isohydric behaviour for that species. Overall, the coherence across findings underscores the robustness of past classifications, even when viewed through the lens of our modernized spectrum of isohydric behaviour.

Coordination of drought response traits

Our results indicate that among the studied tree species, drought response traits are associated in a consistent fashion in line with their theoretically expected sequence (Bartlett et al. 2016). For all species, stomatal closure occurred and, for all species with the exception of *B. pendula*, turgor loss happened before reaching water potentials associated with the onset of embolism formation (P_{12}). This strict avoidance of loss of xylem function has been documented elsewhere (Hochberg et al. 2017, Martin-StPaul et al. 2017, Li et al. 2018) and illustrates the strong selection in favour of trait combinations that protect the functionality of the plant conductive system.

Counter to our expectations, neither embolism resistance nor the associated HSMs were related to metrics of isohydry. Instead, our results indicate traits associated with plant drought response to cluster along two largely independent axes of variation. In our PCA, both HSA and the water potential at 90% loss of stomatal conductance (P_{gs90}) scored strongly on the first axis, which suggests that this axis is linked to the isohydry continuum. Likewise, the unexpected high scores of hydraulic capacitance (C) on that axis further indicate that the position of a species on that axis is associated with drought avoidance traits. The link between C and traits associated with the first phase of plant response to drought is confirmed by the clustered correlation matrix.

The second axis of the PCA was associated with critical embolism thresholds and HSM and can hence be interpreted as an axis of xylem safety. This implies that plants may be able to adjust their drought response along two largely independent axes reflecting different underlying trade-offs rather than reducing to a single axis of variation defining a spectrum of drought tolerance strategies as suggested by Choat et al. (2018). While these results should be interpreted with care due to the low number of species in our dataset, stomatal stringency and xylem resistance to drought-induced embolism formation were largely decoupled. This finding contrasts with many published accounts on the isohydry spectrum (Klein 2014, Martínez-Vilalta et al. 2014, Pivovaroff et al. 2018, Fu and Meinzer 2019), but may reflect the lack of a direct mechanistic link between both sets of characteristics. While a coordination between stomatal response and embolism formation requires stomata to close before the onset of embolism formation (Martin-StPaul et al. 2017), there is no mechanism that dictates how wide the water potential range from stomatal closure to critical hydraulic failure should be for a given P_{gs90} (cf. McCulloh et al. 2019). Hence, potential associations between stomatal sensitivity and xylem vulnerability traits may reflect their independent roles in drought tolerance rather than coordinated function (Bartlett et al. 2016). It is therefore possible that many viable strategies exist that are based on different combinations of stomatal response and xylem resistance traits. Ultimately, studies on larger numbers of species from different biomes are needed to determine the level of integration between these different groups of drought

response traits (Hé et al. 2020), as well as their link to trade-offs associated with other environmental stressors (Puglielli et al. 2021) and main axes of plant trait variation above- (Wright et al. 2004) and belowground (Weemstra et al. 2016).

The temporal progression of plant drought responses

To understand and predict the behaviour of plants under drought, it is therefore paramount to shift the focus from merely comparing critical water potentials to estimating the time it takes to reach them (Arend et al. 2021). Our results illustrate that by separating the total time to hydraulic failure into a component before and a component after stomatal closure, it is possible to gain insights about the coordination of plant drought responses that are not available otherwise. A similar approach has been proposed in the conceptual framework of Hammond and Adams (2019). However, these authors divided the dynamics of plant desiccation into phases based on mortality risk rather than on critical water potentials, with the first phase lasting from the onset of drought to incipient mortality risk (cf. Sapes et al. 2019) and the second phase from this point to the 'point of no return' (defined as a 50% mortality risk; Hammond et al. 2019). As the mortality risk of individual plants is very difficult to quantify (cf. Hajek et al. 2022), in this study we prefer to work with water potential thresholds, which have the additional advantage of being defined in terms of the most important state variable used to describe plant water status (cf. De Swaef et al. 2022). In addition, these definitions allow intuitive interpretations of t_{sc} as the time to stomatal closure and t_{crit} as the time needed to cross the stomatal HSM. As stomatal closure consistently happens before the onset of embolism formation and hence prior to the point of incipient mortality risk (Martin-StPaul et al. 2017, Sperry et al. 2017), the two definitions of the two phases in our study are not identical to those in Hammond and Adams (2019). Thus, the associations between drying times and hydraulic traits observed here partially differ from the trait associations predicted by these authors.

As long as stomata are open, their conductance dwarves cuticular and residual conductance (Duursma et al. 2019) and bark conductance (Wolfe 2020). For that reason, the contribution of the latter to total plant water loss is negligible in the first phase. Consistent with this, we found the standardized time to stomatal closure (t_{sc_stan}) to be more strongly associated with P_{gs90} and the mechanistically closely related water potential at turgor loss point (P_{tlp}) than with cuticular conductance (g_{min}). However, in contrast to our expectations, g_{min} was not associated with the second cluster of the correlation matrix (i.e. the second phase of plant response to drought that contains the standardized drying time after stomatal closure, t_{crit_stan}). Instead, we found that despite its low association with both t_{sc_stan} and t_{crit_stan}, g_{min} was mostly associated to the first phase of plant response to drought. This is possibly due to the relatively low range of g_{min} of 1.28 to 3.33 mmol m^{-2} s^{-1} covered by our dataset compared with the wide range reported for this trait (cf. Duursma et al. 2019). Likewise, based on the model presented in Eq. 1 of Blackman et al. (2019), we expected hydraulic capacitance (C) to be mainly related to the second phase of plant response to drought (i.e. second cluster of our correlation matrix). We assumed that C would primarily buffer the time to critical hydraulic failure. However, while C seems to be linked to both t_{sc_stan} and t_{crit_stan} and to both axes of the PCA, it was mostly associated with the cluster corresponding to the first phase of plant response to drought. Therefore, in our study C seems to mainly play a role in buffering time to stomatal closure.

In addition to these observations. The strong association of t_{crit_stan} with HSM and critical embolism thresholds reinforces its interpretation as the time needed to cross the HSM. Interestingly, the standardized average times plants of a species spent in each of the two phases were correlated neither with each other nor with the average total desiccation time. This illustrates that a focus only on drying times after stomatal closure (cf., Blackman et al. 2016, 2019) may not always be sufficient to predict the time to death of a plant under natural drought conditions and shows that there are multiple strategies for plants to cope with drought that rely on adjustments of different traits.

Conclusions

Our study confirms the hypothesized agreement between the water potential at stomatal closure and the HSA, corroborating the value of the latter as an index of stomatal stringency. Consistent with our assumptions, more isohydric species had larger internal water storage and lost their leaf turgor at less negative water potentials. However, counter to our expectations the degree of isohydry was entirely unrelated to embolism resistance and HSM. The latter formed a separate axis of variation linked to the duration of time from stomatal closure to lethal levels of desiccation, while the traits related to stomatal control as expected were more strongly associated with the time to stomatal closure. Our results highlight the importance of the temporal dynamics of plant drought responses and show that a different set of traits affects drying time before and after stomatal closure. Dividing the entire drought response process into distinct phases associated with distinct processes is paramount for effectively capturing the relationships between hydraulic traits and critical timings. Using an aggregate of the two phases obscures the nuances of these interactions. Moreover, stomatal stringency was largely decoupled from standardized drying time, which illustrates that isohydry alone paints an incomplete picture of plant drought responses. Ultimately, to improve our understanding of the coordination of plant traits and their role in different phases of desiccation, it will be necessary to study whether the observed trait patterns generalize onto larger species samples from different biomes both in-situ and in dry-down experiments under controlled conditions.

Acknowledgments

Logistical and scientific assistance from the University of Würzburg, Germany, is gratefully acknowledged. We thank Christine Gernert and Yvonne Heppenstiel for their skilful support in the laboratory during microscopic work and wood anatomical analyses, and Jutta Winkler-Steinbeck for regular supervision of the plants.

Supplementary data

Supplementary data for this article are available at *Tree Physiology* Online.

Funding

M.K. expresses his gratitude to the Indian Council of Agricultural Research (ICAR), New Delhi, India, for providing financial support through the Netaji Subhas—ICAR International Fellowship Program.

The authors further gratefully acknowledge the financial support granted by the Bundesministerium für Ernährung und Landwirtschaft (Germany), Bundesministerium für Umwelt, Naturschutz und nukleare Sicherheit (Germany) and the Fachagentur Nachwachsende Rohstoffe eV (Germany) within the frame of the "Waldklimafond" (project NONNATIVE) partly funded this study.

Conflict of interest

None declared.

Data availability

All tree level and species level data have been uploaded to the Zenodo database (https://zenodo.org), DOI: 10.5281/zenodo.8117431(https://zenodo.org/record/8117431).

References

Adams HD, Zeppel MJB, Anderegg WRL, Hartmann H, Landhäusser SM, Tissue DT, Huxman TE, Hudson PJ, Franz TE, Allen CD, et al. 2017. A multi-species synthesis of physiological mechanisms in drought-induced tree mortality. Nat Ecol Evol. 1(9):1285–1291. https://doi.org/10.1038/s41559-017-0248-x.

Arend M, Link RM, Patthey R, Hoch G, Schuldt B, Kahmen A. 2021. Rapid hydraulic collapse as cause of drought-induced mortality in conifers. Proc Natl Acad Sci USA. 118(16):e2025251118. https://doi.org/10.1073/pnas.2025251118.

Bartlett M, Scoffoni C, Ardy R, Ya Z, Shanwen S, Cao K-F, Sack L. 2012*a*. Rapid determination of comparative drought tolerance traits: using an osmometer to predict turgor loss point. Methods Ecol Evol. 3(5):880–888. https://doi.org/10.1111/j.2041-210X.2012.00230.x.

Bartlett MK, Scoffoni C, Sack L. 2012*b*. The determinants of leaf turgor loss point and prediction of drought tolerance of species and biomes: a global meta-analysis. Ecol Lett. 15(5):393–405. https://doi.org/10.1111/j.1461-0248.2012.01751.x.

Bartlett MK, Zhang Y, Kreidler N, Sun S, Ardy R, Cao K, Sack L. 2014. Global analysis of plasticity in turgor loss point, a key drought tolerance trait. Ecol Lett. 17(12):1580–1590. https://doi.org/10.1111/ele.12374.

Bartlett MK, Klein T, Jansen S, Choat B, Sack L. 2016. The correlations and sequence of plant stomatal, hydraulic, and wilting responses to drought. Proc Natl Acad Sci USA. 113(46):13098–13103. https://doi.org/10.1073/pnas.1604088113.

Beikircher B, Sack L, Ganthaler A, Losso A, Mayr S. 2021. Hydraulic-stomatal coordination in tree seedlings: tight correlation across environments and ontogeny in *Acer pseudoplatanus*. New Phytol. 232(3):1297–1310. https://doi.org/10.1111/nph.17585.

Blackman CJ, Pfautsch S, Choat B, Delzon S, Gleason SM, Duursma RA. 2016. Toward an index of desiccation time to tree mortality under drought. Plant Cell Environ. 39(10):2342–2345. https://doi.org/10.1111/pce.12758.

Blackman CJ, Li X, Choat B, Rymer PD, De Kauwe MG, Duursma RA, Tissue DT, Medlyn BE. 2019. Desiccation time during drought is highly predictable across species of eucalyptus from contrasting climates. New Phytol. 224(2):632–643. https://doi.org/10.1111/nph.16042.

Brodribb TJ, Cochard H. 2009. Hydraulic failure defines the recovery and point of death in water-stressed conifers. Plant Physiol. 149(1):575–584. https://doi.org/10.1104/pp.108.129783.

Brodribb TJ, McAdam SAM. 2017. Evolution of the stomatal regulation of plant water content. Plant Physiol. 174(2):639–649. https://doi.org/10.1104/pp.17.00078.

Brodribb TJ, Holbrook NM, Edwards EJ, Gutiérrez MV. 2003. Relations between stomatal closure, leaf turgor and xylem vulnerability in eight tropical dry forest trees. Plant Cell Environ. 26(3):443–450. https://doi.org/10.1046/j.1365-3040.2003.00975.x.

Challis A, Blackman C, Ahrens C, Medlyn B, Rymer P, Tissue D. 2022. Adaptive plasticity in plant traits increases time to hydraulic failure under drought in a foundation tree. Tree Physiol. 42(4):708–721. https://doi.org/10.1093/treephys/tpab096.

Chen Z, Zhang Y, Yuan W, Zhu S, Pan R, Wan X, Liu S. 2021. Coordinated variation in stem and leaf functional traits of temperate broadleaf tree species in the isohydric-anisohydric spectrum. Tree Physiol. 41(9):1601–1610. https://doi.org/10.1093/treephys/tpab028.

Choat B, Brodribb TJ, Brodersen CR, Duursma RA, López R, Medlyn BE. 2018. Triggers of tree mortality under drought. Nature. 558(7711):531–539. https://doi.org/10.1038/s41586-018-0240-x.

Cochard H, Damour G, Bodet C, Tharwat I, Poirier M, Améglio T. 2005. Evaluation of a new centrifuge technique for rapid generation of xylem vulnerability curves. Physiol Plant. 124(4):410–418. https://doi.org/10.1111/j.1399-3054.2005.00526.x.

Cochard H, Pimont F, Ruffault J, Martin-StPaul N. 2021. SurEau: a mechanistic model of plant water relations under extreme drought. Annals of Forest Science. 78(2). https://doi.org/10.1007/s13595-021-01067-y.

De Baerdemaeker NJF, Hias N, Van den Bulcke J, Keulemans W, Steppe K. 2018. The effect of polyploidization on tree hydraulic functioning. Am J Bot. 105(2):161–171. https://doi.org/10.1002/ajb2.1032.

De Swaef T, Pieters O, Appeltans S, Borra-Serrano I, Coudron W, Couvreur V, Garré S, Lootens P, Nicolaï B, Pols L, et al. 2022. On the pivotal role of water potential to model plant physiological processes. In Silico Plants. 4(1):diab038. https://doi.org/10.1093/insilicoplants/diab038.

Deutscher Wetterdienst. 2023. Deutscher Wetterdienst. https://www.dwd.de/ (8 December 2023, date last accessed).

Duursma RA, Blackman CJ, Lopéz R, Martin-StPaul NK, Cochard H, Medlyn BE. 2019. On the minimum leaf conductance: its role in models of plant water use, and ecological and environmental controls. New Phytol. 221(2):693–705. https://doi.org/10.1111/nph.15395.

Epila J, De Baerdemaeker NJF, Vergeynst LL, Maes WH, Beeckman H, Steppe K. 2017. Capacitive water release and internal leaf water relocation delay drought-induced cavitation in African *Maesopsis eminii*. Tree Physiol. 37(4):481–490. https://doi.org/10.1093/treephys/tpw128.

Farrell C, Szota C, Arndt SK. 2017. Does the turgor loss point characterize drought response in dryland plants? Plant Cell Environ. 40(8):1500–1511. https://doi.org/10.1111/pce.12948.

Feng X, Ackerly DD, Dawson TE, Manzoni S, McLaughlin B, Skelton RP, Vico G, Weitz AP, Thompson SE. 2019. Beyond isohydricity: the role of environmental variability in determining plant drought responses. Plant Cell Environ. 42(4):1104–1111. https://doi.org/10.1111/pce.13486.

Fu X, Meinzer FC. 2019. Metrics and proxies for stringency of regulation of plant water status (iso/anisohydry): a global data set reveals coordination and trade-offs among water transport traits. Tree Physiol. 39(1):122–134. https://doi.org/10.1093/treephys/tpy087.

Gillner S, Korn S, Hofmann M, Roloff A. 2017. Contrasting strategies for tree species to cope with heat and dry conditions at urban sites. Urban Ecosyst. 20(4):853–865. https://doi.org/10.1007/s11252-016-0636-z.

Graves S, Dorai-Raj H-PP. 2023. multcompView: Visualizations of paired comparisons. https://cran.r-project.org/web/packages/multcompView/index.html (29 June 2023, date last accessed).

Grossiord C, Buckley TN, Cernusak LA, Novick KA, Poulter B, Siegwolf RTW, Sperry JS, McDowell NG. 2020. Plant responses to rising vapor pressure deficit. New Phytol. 226(6):1550–1566. https://doi.org/10.1111/nph.16485.

Hajek P, Link RM, Nock CA, Bauhus J, Gebauer T, Gessler A, Kovach K, Messier C, Paquette A, Saurer M, et al. 2022. Mutually inclusive mechanisms of drought-induced tree mortality. Glob Chang Biol. 28(10):3365–3378. https://doi.org/10.1111/gcb.16146.

Hammond WM, Adams HD. 2019. Dying on time: traits influencing the dynamics of tree mortality risk from drought. Tree Physiol. 39(6):906–909. https://doi.org/10.1093/treephys/tpz050.

Hammond WM, Yu K, Wilson LA, Will RE, Anderegg WRL, Adams HD. 2019. Dead or dying? Quantifying the point of no return from hydraulic failure in drought-induced tree mortality. New Phytol. 223(4):1834–1843. https://doi.org/10.1111/nph.15922.

Hammond WM, Williams AP, Abatzoglou JT, Adams HD, Klein T, López R, Sáenz-Romero C, Hartmann H, Breshears DD, Allen CD. 2022. Global field observations of tree die-off reveal hotter-drought fingerprint for Earth's forests. Nat Commun. 13(1):1761. https://doi.org/10.1038/s41467-022-29289-2.

Hartmann H, Link RM, Schuldt B. 2021. A whole-plant perspective of isohydry: stem-level support for leaf-level plant water regulation. Tree Physiol. 41(6):901–905. https://doi.org/10.1093/treephys/tpab011.

Hé D, Biswas S, Xu M, Yang T, You W, Yan E-R. 2020. The importance of intraspecific trait variability in promoting functional niche dimensionality. Ecography. 44:380–390.

Hochberg U, Windt CW, Ponomarenko A, Zhang Y-J, Gersony J, Rockwell FE, Holbrook NM. 2017. Stomatal closure, basal leaf embolism, and shedding protect the hydraulic integrity of grape stems. Plant Physiol. 174(2):764–775. https://doi.org/10.1104/pp.16.01816.

Hochberg U, Rockwell FE, Holbrook NM, Cochard H. 2018. Iso/anisohydry: a plant-environment interaction rather than a simple hydraulic trait. Trends Plant Sci. 23(2):112–120. https://doi.org/10.1016/j.tplants.2017.11.002.

Kerstiens G. 1996. Cuticular water permeability and its physiological significance. J Exp Bot. 47(12):1813–1832. https://doi.org/10.1093/jxb/47.12.1813.

Kiorapostolou N, Galiano L, von Arx G, Gessler A, Petit G. 2018. Structural and anatomical responses of *Pinus sylvestris* and *Tilia platyphyllos* seedlings exposed to water shortage. Trees. 32(5):1211–1218. https://doi.org/10.1007/s00468-018-1703-2.

Klein T. 2014. The variability of stomatal sensitivity to leaf water potential across tree species indicates a continuum between isohydric and anisohydric behaviours. Funct Ecol. 28(6):1313–1320. https://doi.org/10.1111/1365-2435.12289.

Köcher P, Gebauer T, Horna V, Leuschner C. 2009. Leaf water status and stem xylem flux in relation to soil drought in five temperate broad-leaved tree species with contrasting water use strategies. Ann For Sci. 66(1):101–101. https://doi.org/10.1051/forest/2008076.

Köcher P, Horna V, Leuschner C. 2013. Stem water storage in five coexisting temperate broad-leaved tree species: significance, temporal dynamics and dependence on tree functional traits. Tree Physiol. 33(8):817–832. https://doi.org/10.1093/treephys/tpt055.

Kumar M, Waite P-A, Paligi SS, Schuldt B. 2022. Influence of juvenile growth on xylem safety and efficiency in three temperate tree species. Forests. 13(6):909. https://doi.org/10.3390/f13060909.

Leuschner C. 2020. Drought response of European beech (*Fagus sylvatica* L.)—a review. Perspect Plant Ecol Evol Syst. 47:125576. https://doi.org/10.1016/j.ppees.2020.125576.

Leuschner C, Wedde P, Lübbe T. 2019. The relation between pressure–volume curve traits and stomatal regulation of water potential in five temperate broadleaf tree species. Ann For Sci. 76(2):1–14. https://doi.org/10.1007/s13595-019-0838-7.

Leuschner C, Schipka F, Backes K. 2022. Stomatal regulation and water potential variation in European beech: challenging the iso/anisohydry concept. Tree Physiol. 42(2):365–378. https://doi.org/10.1093/treephys/tpab104.

Li X, Blackman CJ, Choat B, Duursma RA, Rymer PD, Medlyn BE, Tissue DT. 2018. Tree hydraulic traits are coordinated and strongly linked to climate-of-origin across a rainfall gradient. Plant Cell Environ. 41(3):646–660. https://doi.org/10.1111/pce.13129.

Li X, Chris B, Peters J, Choat B, Rymer P, Medlyn B, Tissue D. 2019. More than iso/anisohydry: hydroscapes integrate plant water use and drought tolerance traits in 10 eucalypt species from contrasting climates. Funct Ecol. 33(6):1035–1049. https://doi.org/10.1111/1365-2435.13320.

Li X, Xi B, Wu X, Choat B, Feng J, Jiang M, Tissue D. 2022. Unlocking drought-induced tree mortality: physiological mechanisms to modeling. Front Plant Sci. 13:835921. https://doi.org/10.3389/fpls.2022.835921 (29 June 2023, date last accessed).

R Link. 2020. Corrmorant: flexible correlation matrices based on ggplot2. R package version 0.0.0.9007, http://github.com/r-link/corrmorant (3 March 2024, date last accessed).

Mantova M, Herbette S, Cochard H, Torres-Ruiz JM. 2022. Hydraulic failure and tree mortality: from correlation to causation. Trends Plant Sci. 27(4):335–345. https://doi.org/10.1016/j.tplants.2021.10.003.

Manzi OJL, Bellifa M, Ziegler C, Mihle L, Levionnois S, Burban B, Leroy C, Coste S, Stahl C. 2022. Drought stress recovery of hydraulic and photochemical processes in neotropical tree saplings. Tree Physiol. 42(1):114–129. https://doi.org/10.1093/treephys/tpab092.

Martínez-Vilalta J, Garcia-Forner N. 2017. Water potential regulation, stomatal behaviour and hydraulic transport under drought: deconstructing the iso/anisohydric concept. Plant Cell Environ. 40(6):962–976. https://doi.org/10.1111/pce.12846.

Martínez-Vilalta J, Poyatos R, Aguadé D, Retana J, Mencuccini M. 2014. A new look at water transport regulation in plants. New Phytol. 204(1):105–115. https://doi.org/10.1111/nph.12912.

Martin-StPaul N, Delzon S, Cochard H. 2017. Plant resistance to drought depends on timely stomatal closure. Ecol Lett. 20(11):1437–1447. https://doi.org/10.1111/ele.12851.

McAdam SAM, Brodribb TJ. 2014. Separating active and passive influences on stomatal control of transpiration. Plant Physiol. 164(4):1578–1586. https://doi.org/10.1104/pp.113.231944.

McAdam SAM, Brodribb TJ, Ross JJ. 2016. Shoot-derived abscisic acid promotes root growth. Plant Cell Environ. 39(3):652–659. https://doi.org/10.1111/pce.12669.

McCulloh KA, Domec J-C, Johnson DM, Smith DD, Meinzer FC. 2019. A dynamic yet vulnerable pipeline: integration and coordination of hydraulic traits across whole plants. Plant Cell Environ. 42(10):2789–2807. https://doi.org/10.1111/pce.13607.

McDowell NG, Sapes G, Pivovaroff A, Adams HD, Allen CD, Anderegg WRL, Arend M, Breshears DD, Brodribb T, Choat B, et al. 2022. Mechanisms of woody-plant mortality under rising drought, CO2 and vapour pressure deficit. Nat Rev Earth Environ. 3(5):294–308. https://doi.org/10.1038/s43017-022-00272-1.

Meinzer FC, James SA, Goldstein G, Woodruff D. 2003. Whole-tree water transport scales with sapwood capacitance in tropical forest canopy trees: water transport scales with sapwood properties in tropical trees. Plant Cell Environ. 26(7):1147–1155. https://doi.org/10.1046/j.1365-3040.2003.01039.x.

Meinzer FC, Woodruff DR, Marias DE, Smith DD, McCulloh KA, Howard AR, Magedman AL. 2016. Mapping 'hydroscapes' along the iso- to anisohydric continuum of stomatal regulation of plant water status. Ecol Lett. 19(11):1343–1352. https://doi.org/10.1111/ele.12670.

Moser A, Rötzer T, Pauleit S, Pretzsch H. 2016. The urban environment can modify drought stress of small-leaved lime (*Tilia cordata* mill.) and black locust (*Robinia pseudoacacia* L.). Forests. 7(12):71. https://doi.org/10.3390/f7030071.

Moser-Reischl A, Rahman MA, Pauleit S, Pretzsch H, Rötzer T. 2019. Growth patterns and effects of urban micro-climate on two physiologically contrasting urban tree species. Landsc Urban Plan. 183:88–99. https://doi.org/10.1016/j.landurbplan.2018.11.004.

Nobel PS (2009) Physicochemical and environmental plant physiology, 4th edn. Academic Press, Amsterdam, p 582.

Nolan RH, Gauthey A, Losso A, Medlyn BE, Smith R, Chhajed SS, Fuller K, Song M, Li X, Beaumont LJ, et al. 2021. Hydraulic failure and tree size linked with canopy die-back in eucalypt forest during extreme drought. New Phytol. 230(4):1354–1365. https://doi.org/10.1111/nph.17298.

Nolf M, Creek D, Duursma R, Holtum J, Mayr S, Choat B. 2015. Stem and leaf hydraulic properties are finely coordinated in three tropical rain forest tree species. Plant Cell Environ. 38(12):2652–2661. https://doi.org/10.1111/pce.12581.

Oksanen J, Simpson G, Blanchet F, Kindt R, Legendre P, Minchin P, O'Hara R, Solymos P, Stevens M, Szoecs E, et al. 2022. Vegan: Community ecology package. R package version 2.6-4. https://CRAN.R-project.org/package=vegan (3 March 2024, date last accessed).

Pammenter NW, Vander Willigen C. 1998. A mathematical and statistical analysis of the curves illustrating vulnerability of xylem to cavitation. Tree Physiol. 18(8–9):589–593. https://doi.org/10.1093/treephys/18.8-9.589.

Petek-Petrik A, Petrík P, Lamarque LJ, Cochard H, Burlett R, Delzon S. 2023. Drought survival in conifer species is related to the time required to cross the stomatal safety margin. J Exp Bot. 74(21):6847-6859. https://doi.org/10.1093/jxb/erad352.

Pivovaroff AL, Pasquini SC, De Guzman ME, Alstad KP, Stemke JS, Santiago LS. 2015. Multiple strategies for drought survival among woody plant species. Functional Ecology. Portico. 30(4):517-526. https://doi.org/10.1111/1365-2435.12518.

Pivovaroff AL, Cook VMW, Santiago LS. 2018. Stomatal behaviour and stem xylem traits are coordinated for woody plant species under exceptional drought conditions. Plant Cell Environ. 41(11): 2617–2626. https://doi.org/10.1111/pce.13367.

Puglielli G, Hutchings MJ, Laanisto L. 2021. The triangular space of abiotic stress tolerance in woody species: a unified trade-off model. New Phytol. 229(3):1354–1362. https://doi.org/10.1111/nph.16952.

R Core Team 2021. R: A language and environment for statistical computing. R Foundation for Statistical Computing, Vienna, Austria. https://www.R-project.org/.

Robson TM, Hartikainen SM, Aphalo PJ. 2015. How does solar ultraviolet-B radiation improve drought tolerance of silver birch (*Betula pendula* Roth.) seedlings? Plant Cell Environ. 38(5): 953–967. https://doi.org/10.1111/pce.12405.

Rodriguez-Dominguez CM, Buckley TN, Egea G, de Cires A, Hernandez-Santana V, Martorell S, Diaz-Espejo A. 2016. Most stomatal closure in woody species under moderate drought can be explained by stomatal responses to leaf turgor. Plant Cell Environ. 39(9): 2014–2026. https://doi.org/10.1111/pce.12774.

Rogiers SY, Greer DH, Hatfield JM, Hutton RJ, Clarke SJ, Hutchinson PA, Somers A. 2012. Stomatal response of an anisohydric grapevine cultivar to evaporative demand, available soil moisture and abscisic acid. Tree Physiol. 32(3):249–261. https://doi.org/10.1093/treephys/tpr131.

Rötzer T, Häberle KH, Kallenbach C, Matyssek R, Schütze G, Pretzsch H. 2017. Tree species and size drive water consumption of beech/spruce forests - a simulation study highlighting growth under water limitation. Plant Soil. 418(1–2):337–356. https://doi.org/10.1007/s11104-017-3306-x.

Sack L, Scoffoni C. 2011. Minimum epidermal conductance (gmin, a.k.a. cuticular conductance). https://prometheusprotocols.net/function/gas-exchange-and-chlorophyll-fluorescence/stomatal-and-non-stomatal-conductance-and-transpiration/minimum-epidermal-conductance-gmin-a-k-a-cuticular-conductance/ (8 December 2023, date last accessed).

Salvi AM, Gosetti SG, Smith DD, Adams MA, Givnish TJ, McCulloh KA. 2022. Hydroscapes, hydroscape plasticity and relationships to functional traits and mesophyll photosynthetic sensitivity to leaf water potential in eucalyptus species. Plant Cell Environ. 45(9): 2573–2588. https://doi.org/10.1111/pce.14380.

Sapes G, Roskilly B, Dobrowski S, Maneta M, Anderegg WRL, Martinez-Vilalta J, Sala A. 2019. Plant water content integrates hydraulics and carbon depletion to predict drought-induced seedling mortality. Tree Physiol. 39(8):1300–1312. https://doi.org/10.1093/treephys/tpz062.

Schuldt B, Buras A, Arend M, Vitasse Y, Beierkuhnlein C, Damm A, Gharun M, Grams TEE, Hauck M, Hajek P, et al. 2020. A first assessment of the impact of the extreme 2018 summer drought on central European forests. Basic Appl Ecol. 45:86–103. https://doi.org/10.1016/j.baae.2020.04.003.

Skelton RP, West AG, Dawson TE. 2015. Predicting plant vulnerability to drought in biodiverse regions using functional traits. Proc Natl Acad Sci USA. 112(18):5744–5749. https://doi.org/10.1073/pnas.1503376112.

Sperry JS, Meinzer FC, McCulloh KA. 2008. Safety and efficiency conflicts in hydraulic architecture: scaling from tissues to trees. Plant Cell Environ. 31(5):632–645. https://doi.org/10.1111/j.1365-3040.2007.01765.x.

Sperry JS, Venturas MD, Anderegg WRL, Mencuccini M, Mackay DS, Wang Y, Love DM. 2017. Predicting stomatal responses to the environment from the optimization of photosynthetic gain and hydraulic cost. Plant Cell Environ. 40(6):816–830. https://doi.org/10.1111/pce.12852.

Steppe K, Lemeur R. 2007. Effects of ring-porous and diffuse-porous stem wood anatomy on the hydraulic parameters used in a water flow and storage model. Tree Physiol. 27(1):43–52. https://doi.org/10.1093/treephys/27.1.43.

Tardieu F, Simonneau T. 1998. Variability among species of stomatal control under fluctuating soil water status and evaporative demand: modelling isohydric and anisohydric behaviours. J Exp Bot. 49(Special):419–432. https://doi.org/10.1093/jxb/49.Special_Issue.419.

Trueba S, Pan R, Scoffoni C, John GP, Davis SD, Sack L. 2019. Thresholds for leaf damage due to dehydration: declines of hydraulic function, stomatal conductance and cellular integrity precede those for photochemistry. New Phytol. 223(1):134–149. https://doi.org/10.1111/nph.15779.

Urli M, Porte AJ, Cochard H, Guengant Y, Burlett R, Delzon S. 2013. Xylem embolism threshold for catastrophic hydraulic failure in angiosperm trees. Tree Physiol. 33(7):672–683. https://doi.org/10.1093/treephys/tpt030.

Vergeynst LL, Dierick M, Bogaerts JAN, Cnudde V, Steppe K. 2015. Cavitation: a blessing in disguise? New method to establish vulnerability curves and assess hydraulic capacitance of woody tissues. Tree Physiol. 35(4):400–409. https://doi.org/10.1093/treephys/tpu056.

Vogt UK. 2001. Hydraulic vulnerability, vessel refilling, and seasonal courses of stem water potential of *Sorbus aucuparia* L. and *Sambucus nigra* L. J Exp Bot. 52(360):1527–1536. https://doi.org/10.1093/jexbot/52.360.1527.

Weemstra M, Mommer L, Visser EJW, van Ruijven J, Kuyper TW, Mohren GMJ, Sterck FJ. 2016. Towards a multidimensional root trait framework: a tree root review. New Phytol. 211(4):1159–1169. https://doi.org/10.1111/nph.14003.

Wolfe BT. 2020. Bark water vapour conductance is associated with drought performance in tropical trees. Biol Lett. 16(8):20200263. https://doi.org/10.1098/rsbl.2020.0263.

Wright IJ, Reich PB, Westoby M, Ackerly DD, Baruch Z, Bongers F, Cavender-Bares J, Chapin T, Cornelissen JHC, Diemer M, et al. 2004. The worldwide leaf economics spectrum. Nature. 428(6985):821–827. https://doi.org/10.1038/nature02403.

Yuan W, Zheng Y, Piao S, Ciais P, Lombardozzi D, Wang Y, Ryu Y, Chen G, Dong W, Hu Z, et al. 2019. Increased atmospheric vapor pressure deficit reduces global vegetation growth. Sci Adv. 5(8):eaax1396. https://doi.org/10.1126/sciadv.aax1396.

Zhang Y, Oren R, Kang S. 2012. Spatiotemporal variation of crown-scale stomatal conductance in an arid *Vitis vinifera* L. cv. Merlot vineyard: direct effects of hydraulic properties and indirect effects of canopy leaf area. Tree Physiol. 32(3):262–279. https://doi.org/10.1093/treephys/tpr120.

Ziegler C, Levionnois S, Bonal D, Heuret P, Stahl C, Coste S. 2023. Large leaf hydraulic safety margins limit the risk of drought-induced leaf hydraulic dysfunction in neotropical rainforest canopy tree species. Funct Ecol. 37(6):1717–1731. https://doi.org/10.1111/1365-2435.14325.